Epoxidation of Olefins by $[Ru^{IV}(bpy)_2(py)(O)]^{2+}$ in Acetonitrile Solution. A Global Kinetic Analysis of the Epoxidation of *trans*-Stilbene

Laura K. Stultz, Robert A. Binstead, Martha S. Reynolds,† and Thomas J. Meyer*

Contribution from the Department of Chemistry, University of North Carolina at Chapel Hill, Chapel Hill, North Carolina 27599-3290

Received July 21, 1994. Revised Manuscript Received November 28, 1994®

Abstract: The mechanism of epoxidation of the olefins *cis*- and *trans*-stilbene, styrene, and norbornene by the oxidant $[Ru^{IV}(bpy)_2(py)(O)]^{2+}$ has been investigated in acetonitrile solution by both conventional product analysis (GC-MS and ^1H NMR) and newly developed global kinetic analysis techniques. Under 1:1 stoichiometric reaction conditions (15 mM) the organic products from the oxidations of *cis*- or *trans*-stilbene included unreacted stilbene (>50%), stilbene oxide (<50%), benzophenone (~6%) and trace amounts of diphenylacetaldehyde. In the case of *trans*-stilbene, use of the ^{18}O-labeled oxidant showed that the oxygen atom of its $Ru^{IV}=O^{2+}$ group was the predominant source of the oxygen in the epoxide products and a major contributor to the oxygen content of benzophenone. Under similar conditions, the oxidations of styrene and norbornene gave styrene oxide and *exo*-norbornene oxide as products by ^1H NMR. Kinetic studies were performed under pseudo-first-order conditions with a large excess of the olefins. Factor analysis of UV−vis spectra *vs* time for each reaction revealed the presence of five colored components and four distinct kinetic processes. In the case of *trans*-stilbene, the initial reaction was well-separated from the following steps, allowing a full global kinetic fit to be obtained to a multistep model. The initial stage involved net oxene insertion into the double bond of the olefin to form the Ru(II) epoxide complex, $[Ru^{II}(bpy)_2(py)(epoxide)]^{2+}$, without evidence for an intermediate. This was followed by a competition between its rapid oxidation by $Ru^{IV}=O^{2+}$ and solvolysis by CH_3CN. In the oxidation step both the Ru(III) epoxide and $[Ru^{III}(bpy)_2(py)(OH)]^{2+}$ are formed. Once formed, $Ru^{III}-OH^{2+}$ was found to react further via initial disproportionation to $Ru^{IV}=O^{2+}$ and $Ru^{II}-OH_2^{2+}$. The aqua complex undergoes irreversible solvolysis ($k = 1.66 \times 10^{-3}$ s^{-1} at 25 °C), and $Ru^{IV}=O^{2+}$ produces further epoxidation. The Ru(III) epoxide intermediate appears to release epoxide and undergo reduction to form $[Ru^{II}(bpy)_2(py)(NCCH_3)]^{2+}$ via a pathway first order in complex. The details of the reduction and solvolysis remain unknown. For the initial step to form Ru(II) epoxide, $k = 0.28$ M^{-1} s^{-1} for *trans*-stilbene, and $k = 2.5 \times 10^{-3}$ s^{-1} for *cis*-stilbene at 25 °C. Activation parameters in CH_3CN for *trans*-stilbene were $\Delta H^{\ddagger} = 4.4 \pm 0.1$ kcal mol^{-1} and $\Delta S^{\ddagger} = -46 \pm 0.4$ cal deg^{-1} mol^{-1}, and for *cis*-stilbene $\Delta H^{\ddagger} = 11.9 \pm 0.1$ kcal mol^{-1} and $\Delta S^{\ddagger} = -30.4 \pm 0.3$ cal deg^{-1} mol^{-1}. Additional, non-epoxide products are formed under stoichiometric or near-stoichiometric conditions because of *overoxidation* of the epoxide product. Overoxidation was accompanied by formation of the μ-oxo-bridged dimer, $[Ru^{III}(bpy)_2(py)]_2O^{4+}$. The same products were observed in the stoichiometric oxidation of *trans*-stilbene oxide by $[Ru^{IV}(bpy)_2(py)(O)]^{2+}$ in CH_3CN.

Introduction

Recent advances in the study of the epoxidation of olefins by high-valent metal oxo complexes[1] and oxometalloporphyrin reagents[2] have led to detailed suggestions about how these reactions may occur. Based largely on the results of product analyses, several mechanisms have been proposed for the initial step in which the key redox intermediates involve the formation of (a) metallaoxetanes, (b) π-cation radicals, (c) carbocations, or (d) carbon σ-radicals, as opposed to concerted oxene insertion into the double bond. The various mechanisms have evolved, in part, from a desire to explain the appearance of additional, non-epoxide products via a common intermediate. As pointed out by Ostovic and Bruice,[2a] the non-epoxide products can be readily accommodated by schemes involving further reactions of initial intermediates or reactions operating parallel to epoxidation. Another possibility that has received little attention is that further oxidation of the epoxide itself may lead to additional products, which depend on the nature of both the olefin and the oxidant.

In an earlier study we reported that epoxidations of styrene, *cis*-stilbene, and *trans*-stilbene could be achieved with the oxidant *cis*-$[Ru^{IV}(bpy)_2(py)(O)]^{2+}$ (bpy = 2,2′-bipyridine, py = pyridine).[3] This and related Ru(IV) oxo and Ru(VI) dioxo complexes have proven to be mechanistically versatile oxidants. A number of mechanistic pathways have been identified for these reagents, including O-atom transfer to sulfides[4] and phosphines,[5,6] electrophilic attack on phenols,[7] hydride transfer from alcohols,[8] and proton-coupled electron transfer with hydroquinones.[9] As well, Che and co-workers have investigated

† Current address: Chemistry Department, Colgate University, Hamiton, NY 13346.

® Abstract published in *Advance ACS Abstracts,* January 15, 1995.

(1) (a) Jorgensen, K. A. *Chem. Rev.* **1989**, *89*, 431. (b) Jorgensen, K. A.; Schiott, B. *Chem. Rev.* **1990**, *90*, 1483. (c) Khenkin, A. M.; Hill, C. L. *J. Am. Chem. Soc.* **1993**, *115*, 8178.

(2) (a) Ostovic, D.; Bruice, T. C. *Acc. Chem. Res.* **1992**, *25*, 314. (b) Watanabe, Y.; Groves, J. T. *The Enzymes*; Sigman, D. S., Ed.; Academic Press: New York, 1992; Vol. XX, pp 405−452. (c) Meunier, B. *Chem. Rev.* **1992**, *92*, 1411. (d) Kim, T.; Gholam, A. M.; Liu, J.; Bauld, N. L. *J. Am. Chem. Soc.* **1993**, *115*, 7653. (e) Arasasingham, R. D.; He, G. X.; Bruice, T. C. *J. Am. Chem. Soc.* **1993**, *115*, 7985.

(3) Dobson, J. C.; Seok, W. K.; Meyer, T. J. *Inorg. Chem.* **1986**, *25*, 1325.

(4) (a) Roecker, L.; Dobson, J. C.; Vining, W. J.; Meyer, T. J. *Inorg. Chem.* **1987**, *26*, 779. (b) Acquaye, J. H.; Muller, J. G.; Takeuchi, K. J. *Inorg. Chem.* **1993**, *32*, 160.

(5) Moyer, B. A.; Sipe, B. K.; Meyer, T. J. *Inorg. Chem.* **1981**, *20*, 1475.

(6) Dovletoglou, A.; Meyer, T. J. *J. Am. Chem. Soc.* **1994**, *116*, 215.

(7) Seok, W. K.; Meyer, T. J. *J. Am. Chem. Soc.* **1988**, *110*, 7358.

(8) (a) Roecker, L.; Meyer, T. J. *J. Am. Chem. Soc.* **1987**, *109*, 746. (b) Marmion, M. E.; Takeuchi, K. J. *J. Chem. Soc., Dalton Trans.* **1988**, 2385. (c) Muller, J. G.; Acquaye, J. H.; Takeuchi, K. J. *Inorg. Chem.* **1992**, *31*, 4552.

0002-7863/95/1517-2520$09.00/0

the epoxidation of olefins with macrocyclic Ru(IV) oxo and Ru(VI) dioxo complexes.[10]

In this work we describe kinetic results pertaining to the epoxidations of the olefins *trans*-stilbene, *cis*-stilbene, styrene, and norbornene, together with a detailed mechanistic study of the epoxidation of *trans*-stilbene based on a global kinetic analysis methodology. There is evidence from these results for complex, multistep reactions, well-defined intermediates, and overoxidation of the epoxide products, which may have important implications for the mechanism of epoxidation with related oxidants such as oxometalloporphyrins and the cytochrome P450 oxidase enzymes.

Experimental Section

Materials. High-purity acetonitrile was used as received from Burdick & Jackson. House-distilled water was purified by use of a Barnstead E-Pure deionization system. ^{18}O-enriched water was purchased from Cambridge Isotope Laboratories and was determined to be 66−70% isotopically labeled by GC-MS analysis. High-purity NMR solvents also were obtained from Cambridge Isotope Laboratories and used as received. The olefins used in the epoxidation studies were obtained from Aldrich Chemical Co. and were purified as follows: *trans*-stilbene (recrystallization twice from ethanol); *cis*-stilbene and styrene (vacuum distillation); and norbornene (sublimation). Ceric perchlorate solution (0.50 N Ce(IV) in 6 N perchloric acid) was purchased from GFS Chemicals and used as received. Common laboratory chemicals employed in the preparation of the compounds were reagent grade and were used without further purification.

Preparations. The salts $[Ru(bpy)_2(py)(OH_2)](PF_6)_2 \cdot H_2O$, $[Ru(bpy)_2(py)(O)](PF_6)_2$, $[Ru(bpy)_2(py)(OH_2)](ClO_4)_2 \cdot H_2O$, and $[Ru(bpy)_2(py)(O)](ClO_4)_2$ were prepared by literature methods.[11,12] ***Caution!*** Although the preparations of the perchlorate salts described here have been repeated numerous times without incident, particular care should be exercised in the preparation and handling of these compounds. Perchlorate salts of organometallic cations, metal complexes, and organic cations have been known to explode spontaneously. Hexafluorophosphate was used as the counterion except when solubility required the use of a perchlorate salt.

$[Ru(bpy)_2(py)(^{18}O)](ClO_4)_2$. This procedure is a modification of a method described previously.[11] Freshly prepared $[Ru(bpy)_2(py)(OH_2)](ClO_4)_2$ (40 mg) was stirred in 3 g of 66−70% ^{18}O-labeled water for 20 h at room temperature under a nitrogen atmosphere. The solution was filtered and then 0.25 mL of Ce(IV) (0.5 N in 6 M $HClO_4$) was added to the filtrate. The solution turned yellow/green and a precipitate began to form. The mixture was cooled in an ice bath for 10−15 min and the solid $[Ru(bpy)_2(py)(^{18}O)](ClO_4)_2$ was filtered off. The product was washed with a minimum volume of ice cold water and stored in a vacuum dessicator overnight. The product was determined to be 64% ^{18}O-labeled by FTIR, $\nu_{Ru=O} = 792\ cm^{-1}$ (^{16}O), 766 cm^{-1} (^{18}O).[11] It is recommended that the compound be used immediately since the ^{18}O-label can exchange with atmospheric water. This process is slowed by storage in a vacuum desiccator.

Instrumentation. Organic products from the epoxidation reactions were analyzed by use of a Hewlett-Packard 5890 Series II gas chromatograph with a 12 m × 0.2 mm × 0.33 μm HP-1 column (cross-linked methyl silicone gum) and a Hewlett-Packard 5971 A mass selective detector, both interfaced with an HP Vectra PC computer system. ^1H NMR spectra of the products also were obtained in CD_3CN *vs* TMS from a Bruker AC 200 MHz FT-NMR spectrometer. IR spectra were recorded by use of a Mattson Galaxy 5020 series FT-IR spectrophotometer interfaced with an IBM compatible PC. IR measurements were made either in KBr pellets or in CD_3CN solution by use of a demountable cell with NaCl plates and Teflon spacers. Kinetic studies with this cell were performed with a manually operated mixing apparatus consisting of Hamilton gas-tight syringes and a T-valve mixer connected to the solution IR cell with PTFE tubing.

UV−vis spectra were collected as a function of time by use of a Hewlett-Packard 8452A diode array spectrophotometer interfaced with an IBM compatible PC. The measurements were made either in standard 1 cm quartz cuvettes (NSG) or in a solution IR cell (see above) when short path lengths were required. The temperature of solutions during kinetic studies was maintained to within ±0.2 °C with use of a Lauda RM6 circulating water bath and monitored with an Omega HH-51 thermocouple probe. For rapid reactions, UV−vis spectral changes were followed by use of an OLIS (Bogart, GA) RSM/1000 rapid-scanning, dual-beam spectrophotometer linked by a liquid light guide to a Hi-Tech Scientific (Salisbury, England) SF-51 stopped-flow mixing apparatus. The temperature of the reactant solutions was controlled to within ±0.2 °C by use of a Neslab RTE-110 water bath and monitored via the Pt resistance thermometer of the SF-51 apparatus.

Quenching Studies. The presence of Ru(III) intermediates during the epoxidation of *trans*-stilbene by $Ru^{IV}{=}O^{2+}$ in CH_3CN was investigated by monitoring the UV−vis spectral changes after quenching reaction mixtures at various times by the addition of either hydroquinone or ascorbic acid. Both reductants rapidly reduce any Ru(IV) or Ru(III) species to their corresponding Ru(II) forms, which are more easily detected by their characteristic MLCT absorption bands and their different rates of solvolysis to give $[Ru^{II}(bpy)_2(py)(NCCH_3)]^{2+}$.

With hydroquinone as the reducing agent, quenching was effected by manual injection of the reductant solution ($[QH_2]_0 = 2 - 10[Ru]_0$) directly into the observation cell containing the reaction mixture and the subsequent spectral changes were monitored with the HP 8452A diode array. Ascorbic acid reductions were more rapid and required stopped-flow mixing techniques. In these studies, solutions of $Ru^{IV}{=}O^{2+}$ (1×10^{-4} M) and *trans*-stilbene (0.10 M) were brought to constant temperature and mixed in a 1:1 ratio to initiate the reaction. The reaction mixture was loaded rapidly into one syringe of the SF-51 stopped-flow mixing apparatus and quenched by 1:1 mixing with a saturated solution of ascorbic acid at intervals from 1 to 5 min after initiation of the reaction. The rapid spectral changes which ensued were monitored by use of the OLIS RSM/1000 rapid-scanning system. In subsequent reactions, the ascorbic acid solution was diluted by a factor of 2 in order to ascertain whether Ru(III) intermediates were still present after the mixing dead-time of the SF-51 apparatus.

Global Kinetic Analysis. In all cases spectral−kinetic data were processed by use of the program SPECFIT (Spectrum Software Associates, Chapel Hill, NC), which is based on the published works of Zuberbühler *et al.*[13] This program uses the method of Singular Value Decomposition (SVD) to reduce the wavelength−time spectral data matrix (**Y**) to the factor analytical form, $\mathbf{Y} = \mathbf{USV}^t$, where **U** and **V** are sets of orthogonal (linearly independent) *evolutionary* and *spectral* eigenvectors, respectively, and **S** is a set of singular (weighting) factors. In principle, there will be as many eigenvectors as there are spectra or abscissa points in each spectrum, whichever is the smaller.[14] However, one of the advantages of the SVD is that there will be only a small number of *significant* eigenvectors containing *all* of the spectral and evolutionary information from the original set of scans. The remaining eigenvectors contain only experimental noise and can be eliminated from further consideration without loss of information.

Subsequently, the eigenvectors are applied within a global multivariate least-squares regression method (Levenberg−Marquardt) to fit the projection ($\mathbf{Y}' = \mathbf{US}$) of the multiwavelength kinetic data in the subspace spanned by **V** to an appropriate model for $\mathbf{Y} = \mathbf{CA}$, where the matrix **C** contains the concentration profiles and **A** represents the molar absorptivity spectra. The concentration profiles for complex kinetic systems are solved within SPECFIT by numerical integration of a user-defined set of differential rate equations. The numerical integration routines follow accepted methods for solving stiff differential kinetic systems, which are available from a number of literature sources

(9) Binstead, R. A.; McGuire, M. E.; Dovletoglou, A.; Seok, W. K.; Roecker, L.; Meyer, T. J. *J. Am. Chem. Soc.* **1992**, *114*, 173.

(10) (a) Leung, W. H.; Che, C. M. *J. Am. Chem. Soc.* **1989**, *111*, 8812. (b) Che, C. M.; Li, C. K.; Tang, W. T.; Yu, W. Y. *J. Chem. Soc., Dalton Trans.* **1992**, 3153.

(11) Moyer, B. A.; Meyer, T. J. *Inorg. Chem.* **1981**, *20*, 436.

(12) Dobson, J. C.; Helms, J. H.; Doppelt, P.; Sullivan, B. P.; Hatfield, W. E.; Meyer, T. J. *Inorg. Chem.* **1989**, *28*, 2200.

(13) (a) Gampp, H.; Maeder, M.; Meyer, C. J.; Zuberbühler, A. D. *Talanta* **1985**, *32*, 95. (b) Gampp, H.; Maeder, M.; Meyer, C. J.; Zuberbühler, A. D. *Talanta* **1985**, *32*, 257. (c) Maeder, M.; Zuberbühler, A. D. *Anal. Chem.* **1990**, *62*, 2220.

(14) Malinowski, E. R. *Factor Analysis in Chemistry*, 2nd ed.; Wiley-Interscience: New York, 1991.

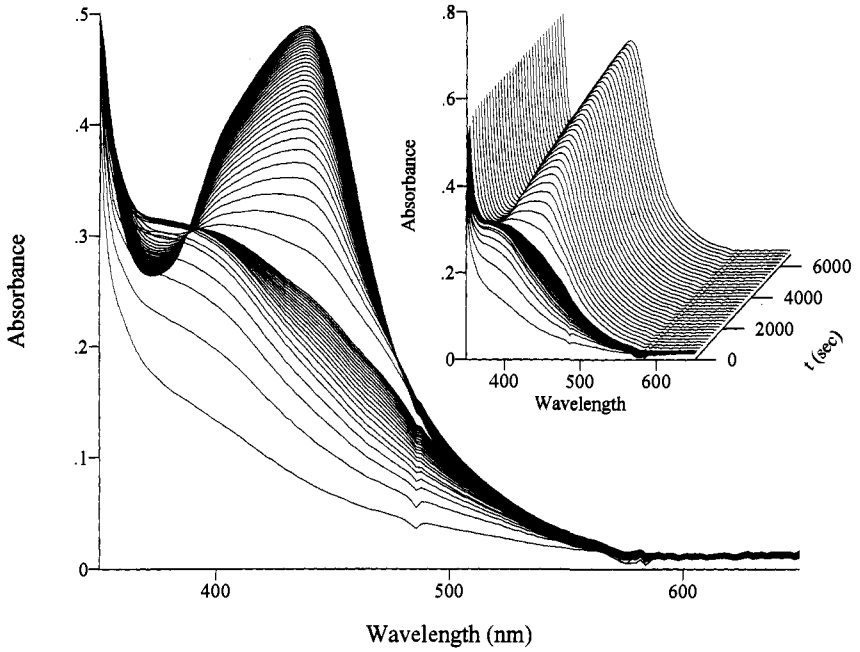

Figure 1. UV−vis spectral changes observed for the reaction of 6.4×10^{-5} M $[Ru^{IV}(bpy)_2(py)(O)]^{2+}$ with 0.080 M *trans*-stilbene in CH_3CN solution at $T = 25 \pm 0.2$ °C, path length = 1.0 cm. For clarity, the initial stage of the reaction is shown with 10 s time steps between traces, while the latter stage is depicted with 200 s time steps.

including the readily accessible book by Press *et al.*[15] The results of such kinetic fits return both globally optimized rate constants and predicted spectra of the colored species. Where necessary, the program was used with known molar absorptivity spectra of some species in order to constrain the fit and thereby return more reliable spectra for those predicted from the fit. In cases of pre-equilibria or unavoidable time delays between initiation of a reaction and the first spectral measurements, the numerical integration routines were used to obtain the reagent concentrations at the time of the initial observation. Where refinement of the rate constants for the initial stage of the model was required to define the starting concentrations accurately, the simulation and parameter refinements were performed repeatedly in order to obtain an acceptable fit at the first observation.

Results

Spectral Changes. In Figure 1 are shown the UV−vis spectral changes with time for the reaction between $[Ru^{IV}(bpy)_2(py)(O)]^{2+}$ (6.4×10^{-5} M) and *trans*-stilbene (80 mM) in CH_3CN at 25 °C. At early times (<60 s), $Ru^{IV}{=}O^{2+}$ disappears with concurrent growth of a new spectral feature near 380 nm, which is very similar to the LMCT transition of $[Ru^{III}(bpy)_2(py)(OH)]^{2+}$ (λ_{max} = 380 nm, ϵ = 5520 M^{-1} cm^{-1}) in CH_3CN.[16] This feature is replaced over a period of several hours with the characteristic spectrum of the solvento complex, $[Ru^{II}(bpy)_2(py)(NCCH_3)]^{2+}$. However, singular value decomposition (SVD) of the data set revealed that the overall reaction was far more complicated. As shown in Figure 2, the SVD revealed the presence of five significant spectral and time domain eigenvectors, corresponding to four distinct kinetic processes. The sixth spectral eigenvector (**V**) was consistent with the line spectrum of the deuterium lamp source of the HP 8452A diode array spectrophotometer and the corresponding temporal changes (**U** × **S**) most likely arise from changes in lamp intensity. The remaining eigenvectors contained only random noise that could be factored from the data.

The nature of the apparent Ru(III) intermediate was investigated by reduction of the reaction mixture with excess hydroquinone (QH_2), as detailed in the Experimental Section. The UV−vis spectral changes following addition of a 10-fold excess of hydroquinone are depicted in Figure 3. Singular value decomposition of the data set revealed the presence of three colored components and the data *appeared* to be consistent with the kinetic model (A → C, B → C) for parallel, first-order solvolysis of two separate Ru(II) complexes. A global fit to this model returned the rate constants $k_A = (2.38 \pm 0.06) \times 10^{-2}$ s^{-1} and $k_B = (1.71 \pm 0.01) \times 10^{-3}$ s^{-1}, the latter being in satisfactory agreement with the value of $k = (1.66 \pm 0.02) \times 10^{-3}$ s^{-1} obtained for the solvolysis of $[Ru^{II}(bpy)_2(py)(OH)_2]^{2+}$ by CH_3CN at 25 °C.[16] A similar result was obtained when only a 2-fold excess of hydroquinone was used, except that the faster of the two rate constants was found to depend on the $[QH_2]$. Since $Ru^{III}{-}OH^{2+}$ is reduced very rapidly by QH_2 ($Ru^{III}{-}OH^{2+} + {}^1/_2QH_2 \rightarrow Ru^{II}{-}OH_2^{2+} + {}^1/_2Q$, $k \sim 1 \times 10^6$ M^{-1} s^{-1}),[9] this behavior indicates that there is yet another Ru(III) intermediate present in the reaction mixture, possibly a Ru(III) epoxide complex. Furthermore, the fact that the SVD did not reveal the presence of any other intermediates following reduction suggests that solvolysis of $Ru^{II}(epoxide)^{2+}$ by CH_3CN must be much faster than the rate of reduction in these experiments. Having established that one of the species present was $[Ru^{II}(bpy)_2(py)(OH_2)]^{2+}$, formed by reduction of either $Ru^{IV}{=}O^{2+}$ or $Ru^{III}{-}OH^{2+}$, the results of the quenching experiments can be explained according to the reaction scheme in eq 1, with the observed rate constant $k_A = k_{red}[QH_2]$ and $k_{solv} \gg k_A$.

$$[Ru^{III}(bpy)_2(py)(epoxide)]^{3+} \xrightarrow[QH_2]{k_A} [Ru^{II}(bpy)_2(py)(epoxide)]^{2+} \quad (1a)$$

$$[Ru^{II}(bpy)_2(py)(epoxide)]^{2+} + CH_3CN \xrightarrow{k_{solv}} [Ru^{II}(bpy)_2(py)(NCCH_3)]^{2+} + \text{epoxide} \quad (1b)$$

$$[Ru^{II}(bpy)_2(py)(OH_2)]^{2+} + CH_3CN \xrightarrow{k_B} [Ru^{II}(bpy)_2(py)(NCCH_3)]^{2+} + H_2O \quad (1c)$$

(15) Press, W. H. *Numerical Recipies in FORTRAN*; Cambridge University Press: New York, 1992.

(16) Binstead, R. A.; Stultz, L. K.; Meyer, T. J. *Inorg. Chem.* **1995**, *34*, 546.

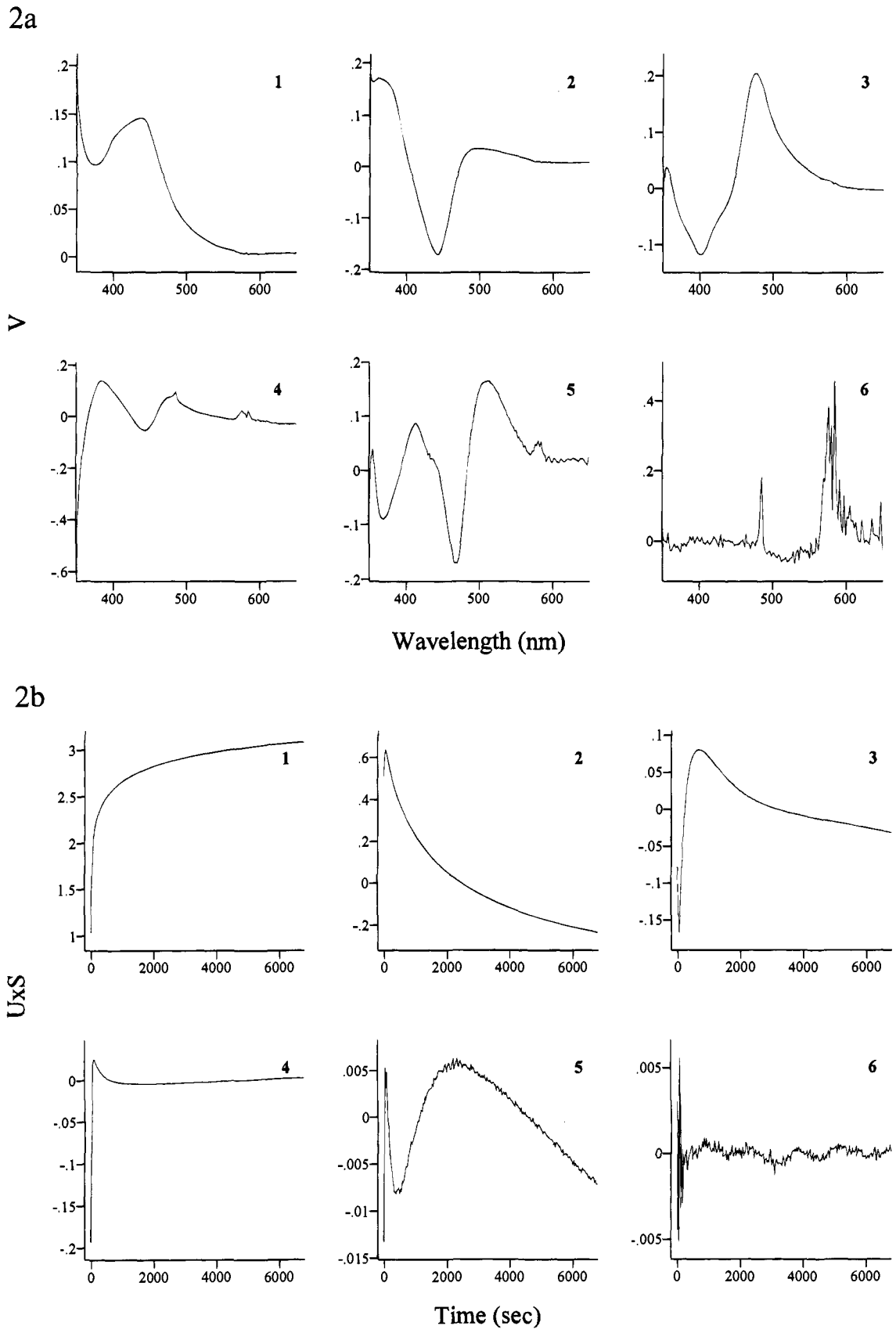

Figure 2. Singular value decomposition of the spectral–kinetic data matrix **Y** in Figure 1 for the reduction of $[Ru^{IV}(bpy)_2(py)(O)]^{2+}$ by *trans*-stilbene showing (a) the first six spectral eigenvectors **V** and (b) the first six temporal eigenvectors from **U** × **S**. (By definition, the data can be reconstructed from the eigenvectors as $\mathbf{Y} \simeq \mathbf{USV}^t$.)

As well as kinetic information, the global fit returned predicted spectra for the three colored components observed during the reduction and solvolysis of the intermediates. With independent knowledge of the spectra of $[Ru^{II}(bpy)_2(py)(OH_2)]^{2+}$ ($\lambda_{max} = 468$ nm, $\epsilon = 8750\ M^{-1}\ cm^{-1}$) and $[Ru^{II}(bpy)_2(py)(NCCH_3)]^{2+}$ ($\lambda_{max} = 440$ nm, $\epsilon = 8160\ M^{-1}\ cm^{-1}$) in CH_3CN,[16] it was possible to determine that ~62% of the $[Ru]_{total}$ appeared initially as $Ru^{II}-OH_2^{2+}$, independent of $[QH_2]$. The

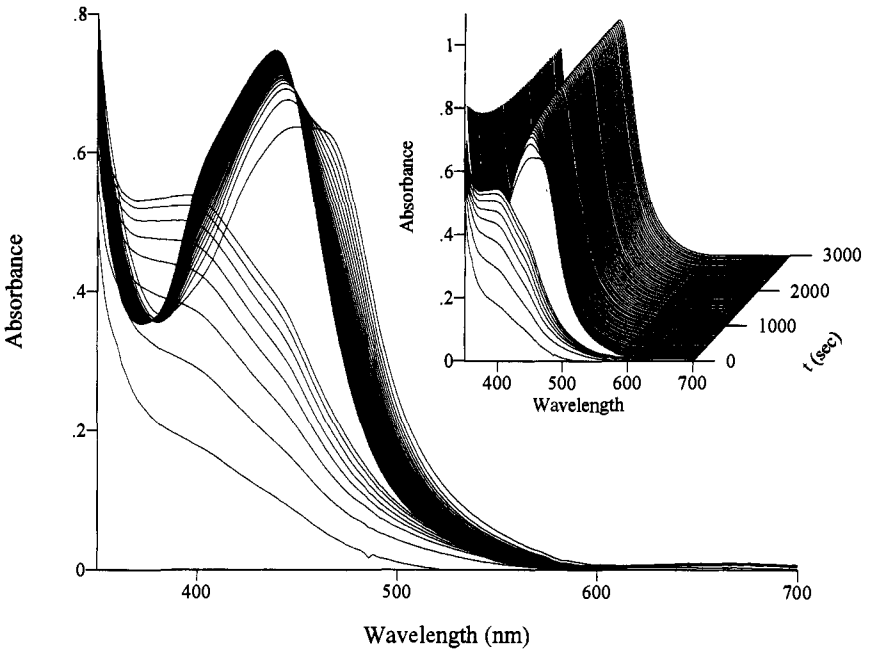

Figure 3. UV−vis spectral changes observed before and after quenching the reaction between 1.0×10^{-4} M $[Ru^{IV}(bpy)_2(py)(O)]^{2+}$ and 0.050 M *trans*-stilbene in CH_3CN solution at $T = 25 \pm 0.2$ °C with a 10-fold excess of hydroquinone, path length = 1.0 cm. The quenching was performed after 63 s and the first observation following reduction was made at 72 s with $[Ru]_{total} = 9.1 \times 10^{-5}$ M. For clarity, the data are depicted with 9 s time steps before quenching and 45 s time steps following quenching.

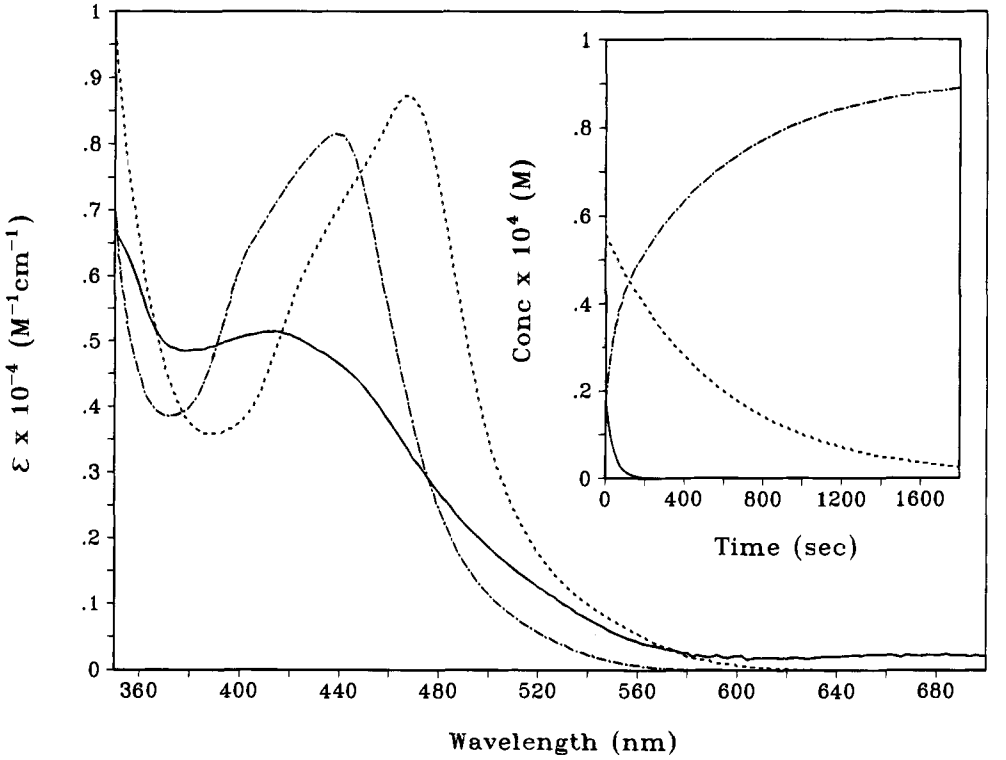

Figure 4. Predicted UV−vis molar absorptivity spectra for $[Ru^{III}(bpy)_2(py)(O\text{-stilbene})]^{3+}$ (—), $[Ru^{II}(bpy)_2(py)(OH_2)]^{2+}$ (- - -) and $[Ru^{II}(bpy)_2(py)(NCCH_3)]^{2+}$ (— • —) in CH_3CN at $T = 25.0 \pm 0.2$ °C obtained from the quenching of the reaction between $[Ru^{IV}(bpy)_2(py)(O)]^{2+}$ and *trans*-stilbene by hydroquinone in Figure 3. (Inset: Concentration profiles obtained from the global fit to the biexponential kinetic model.)

remainder appeared to be a mixture of $Ru^{III}(epoxide)^{3+}$ and $Ru^{II}-NCCH_3^{2+}$. An estimate of the spectrum of $Ru^{III}(epoxide)^{3+}$ was obtained by varying the proportion of $Ru^{II}-NCCH_3^{2+}$ until its characteristic MLCT band no longer appeared in the predicted spectrum of species A in the global fit. The spectra and concentration profiles obtained with the assumption of an initial 1:1 mixture of $Ru^{III}(epoxide)^{3+}$ and $Ru^{II}-NCCH_3^{2+}$ are shown in Figure 4. The small fraction of $Ru^{III}(epoxide)^{3+}$ formed explains the observed pseudo-first-order kinetic behavior with only a 2-fold excess of QH_2 reductant. In this case, the ratio of $[QH_2]:[Ru^{III}(epoxide)^{3+}]$ after reduction of $Ru^{III}-OH^{2+}$ and unreacted $Ru^{IV}=O^{2+}$ was approximately 7.5:1 (15:1 in redox equivalents), sufficiently high to give exponential kinetics for subsequent reduction and rapid solvolysis of $Ru^{III}(epoxide)^{3+}$.

When ascorbic acid was used as the reducing agent, the rate of reduction of the Ru(III) epoxide intermediate was more rapid and had to be followed by the use of stopped-flow mixing. In

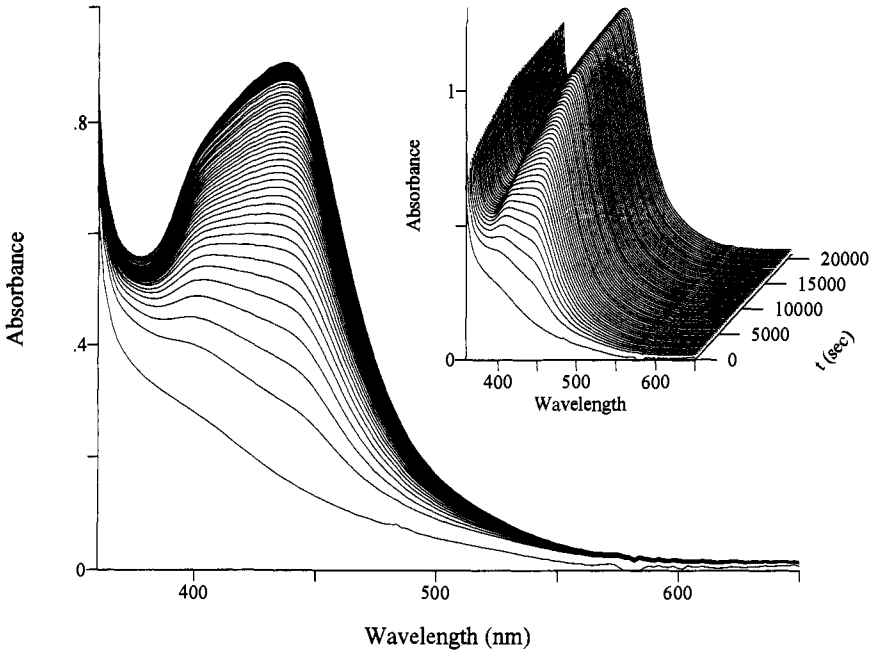

Figure 5. UV−vis spectral changes observed for the reaction between 1.0×10^{-4} M $[Ru^{IV}(bpy)_2(py)(O)]^{2+}$ and 0.250 M *cis*-stilbene in CH_3CN solution at $T = 25.0 \pm 0.2$ °C, path length = 1.0 cm. For clarity, one-tenth of the collected data are depicted with 300 s time steps between traces.

this case, the reduction appeared to be sufficiently rapid that $k'_A > k_{solv}$. The SVD of the rapid-scan spectra revealed the presence of an intermediate, presumed to be the Ru(II) epoxide complex, before solvolysis occurred to give $Ru^{II}-NCCH_3^{2+}$. The data analysis was complicated by the small amount of Ru^{II}-(epoxide)$^{2+}$ formed, the small absorbance changes, and the poorer S/N ratio of the rapid-scan data. The same biexponential kinetic model was applied but with a fixed rate constant for k_B. The global fits for 16 determinations returned an average value of $k_{solv} = 0.42 \pm 0.05$ s^{-1}. There was no significant dependence of the observed rate constant on the concentration of ascorbic acid over a 2-fold range, indicating that this was indeed the solvolysis step for $Ru^{II}(epoxide)^{2+}$.

The appearance of $Ru^{II}-OH_2^{2+}$ in solutions quenched by hydroquinone and ascorbic acid is to be expected as it is the product of reduction of $Ru^{IV}=O^{2+}$ or $Ru^{III}-OH^{2+}$ by hydroquinone in CH_3CN.[9] The relatively large amount (~62%) of the aqua complex comes from two sources: (a) approximately 30% of the initial $Ru^{IV}=O^{2+}$ was unreacted at the time of quenching (60 s) based on a kinetic simulation of the proposed kinetic model (see Discussion); and (b) the remainder is produced by reduction of the Ru(III) hydroxo complex. The presence of $Ru^{III}-OH^{2+}$, as evidenced by the appearance of a small spectral feature near 470 nm at early times during epoxidation (Figure 1), causes a further complication due to its disproportionation equilibrium (eq 2) and solvolysis of $Ru^{II}-OH_2^{2+}$ (eq 1c), which have been studied independently.[16]

$$2[Ru^{III}(bpy)_2(py)(OH)]^{2+} \underset{}{\overset{K_{disp} = 0.02}{\rightleftharpoons}} [Ru^{IV}(bpy)_2(py)(O)]^{2+} + [Ru^{II}(bpy)_2(py)(OH_2)]^{2+} \quad (2)$$

Once formed, $Ru^{IV}=O^{2+}$ undergoes further reaction with excess olefin via the same steps as at early times. In all cases, $Ru^{II}-NCCH_3^{2+}$ appears as the final product. It appears by solvolysis via four distinct pathways: (a) from a Ru(II) epoxide complex formed *prior* to quenching; (b) from $Ru^{II}-OH_2^{2+}$ formed *prior* to quenching via disproportionation of $Ru^{III}-OH^{2+}$; (c) from reduction and solvolysis of a Ru(III) epoxide complex; and (d) from $Ru^{II}-OH_2^{2+}$ following reduction of unreacted $Ru^{IV}=O^{2+}$ and any $Ru^{III}-OH^{2+}$ formed during the course of the reaction. The relatively large fraction of $Ru^{II}-NCCH_3^{2+}$ assumed to be present immediately after quenching (Figure 4) is a result of contributions from pathways (a) and (b), and the spectral traces obtained prior to quenching (Figure 3) show evidence for the presence of the solvento complex even at very early times. The appearance of Ru(III) in the initial stage of epoxidation as $Ru^{III}-OH^{2+}$ and $Ru^{III}(epoxide)^{3+}$ can be explained by pseudo-comproportionation (eq 3) between $Ru^{IV}=O^{2+}$ and Ru^{II}-(epoxide)$^{2+}$.

$$Ru^{IV}=O^{2+} + Ru^{II}(epoxide)^{2+} + H_2O \rightarrow Ru^{III}-OH^{2+} + Ru^{III}(epoxide)^{3+} + OH^- \quad (3)$$

The slow spectral changes that occur past 60 s in Figure 1 can be accounted for largely by rate-limiting disproportionation of $Ru^{III}-OH^{2+}$ ($k \sim 80$ M^{-1} s^{-1}). However, the SVD of the data set demonstrates that another form of Ru(III) must also be present during this stage of the reaction. By inference, this component is also $Ru^{III}(epoxide)^{3+}$. The second set of color changes during this stage of the reaction can be attributed to reduction of $Ru^{III}(epoxide)^{3+}$ to give $Ru^{II}-NCCH_3^{2+}$ or by reduction followed by solvolysis. Although the overall reaction must involve six different complexes, only five are ever present at observable concentrations since $Ru^{II}(epoxide)^{2+}$ is rapidly lost via oxidation by $Ru^{IV}=O^{2+}$ and solvolysis by CH_3CN. As $Ru^{IV}=O^{2+}$ becomes depleted, its reaction with $Ru^{II}(epoxide)^{2+}$ (eq 3) slows and the solvolysis reaction becomes a major source for the appearance of free epoxide in the solution.

In Figure 5 are shown the corresponding UV−vis spectral changes with time for the reaction between $[Ru^{IV}(bpy)_2(py)$-$(O)]^{2+}$ (1.0×10^{-4} M) and *cis*-stilbene (250 mM) in CH_3CN at 25 °C. In comparison to *trans*-stilbene there are two notable observations. The first is that the initial disappearance of $Ru^{IV}=O^{2+}$ is considerably slower despite a substantially higher concentration of olefin in this case. This results in temporal superposition of the initial Ru(IV) → Ru(III) and subsequent Ru(III) → Ru(II) stages of the reaction. The second is that the time scale for the Ru(III) → Ru(II) stage is comparable for either olefin. In the case of styrene or norbornene, the first stage of the reaction is also much slower relative to *trans*-stilbene, while the final stage remains relatively independent of olefin. The

Table 1. Product Analyses by GC-MS for Oxidations by $[Ru^{IV}(bpy)_2(py)(O)]^{2+}$ in CH_3CN

reaction	stoichiometry	products	ratio, %
$Ru^{IV}=O^{2+}$ + *trans*-stilbene	1:1	*trans*-stilbene	44
		trans-stilbene oxide	49
		benzophenone	5.5
		diphenylacetaldehyde	trace
	2:1	*trans*-stilbene	8
		trans-stilbene oxide	79
		benzophenone	13
		diphenylacetaldehyde	trace
	1:2	*trans*-stilbene	72
		trans-stilbene oxide	24
		benzophenone	4
		diphenylacetaldehyde	trace
$Ru^{IV}=O^{2+}$ + *trans*-stilbene (argon purged)	1:1	*trans*-stilbene	58
		trans-stilbene oxide	39
		benzophenone	3
		diphenylacetaldehyde	trace
$Ru^{III}-OH^{2+}$ + *trans*-stilbene[a]	1:1	*trans*-stilbene	78
		trans-stilbene oxide	21
		benzophenone	3
		diphenylacetaldehyde	trace
$Ru^{IV}=O^{2+}$ + *cis*-stilbene	1:1	*cis*-stilbene	55
		cis-stilbene oxide	40
		trans-stilbene oxide	2
		benzophenone	3
		diphenylacetaldehyde	trace
$Ru^{IV}=O^{2+}$ + *cis*-stilbene (argon purged)	1:1	*cis*-stilbene	62
		cis-stilbene oxide	30
		trans-stilbene oxide	3
		trans-stilbene	trace
		benzophenone	2
		diphenylacetaldehyde	trace
$Ru^{IV}=O^{2+}$ + *trans*-stilbene oxide	1:1	benzophenone	6
		diphenylacetaldehyde	10
		trans-stilbene oxide	84

[a] Note that $Ru^{III}-OH^{2+}$ appears to serve *only* as a source of $Ru^{IV}=O^{2+}$ via disproportionation. This is consistent with the similarity in product distribution for oxidation of *trans*-stilbene by $Ru^{IV}=O^{2+}$ under 1 (Ru):2(stilbene) conditions.

temporal overlap in these cases makes it difficult to extract kinetic data as detailed as those obtained with *trans*-stilbene. However, SVD analyses revealed the presence of five colored components and four distinct kinetic processes over the time course of these reactions as well.

Organic Product Analysis and Stoichiometry. In order to determine the nature of the organic products in the reactions between $Ru^{IV}=O^{2+}$ and *cis*- or *trans*-stilbene in CH_3CN, GC-MS analysis was performed on mixtures obtained after reaction for ~20 h at room temperature. Unlike the kinetics experiments, the product analyses were determined from reactions performed close to stoichiometric conditions in order to determine product ratios accurately. The product distributions obtained at Ru:olefin ratios of 1:2, 1:1, and 2:1 are listed in Table 1. They show that in addition to the epoxide, benzophenone and trace amounts of diphenylacetaldehyde were also produced, but not the corresponding diphenyl acetic acid. Note that the use of $Ru^{III}-OH^{2+}$ leads to the same products but in half the yield, indicating that the only role served by this oxidant is as a source of $Ru^{IV}=O^{2+}$ via disproportionation (see above).

In the case of *trans*-stilbene, epoxide was formed in approximately half the amount expected for stoichiometric epoxidation. In the absence of oxygen a slight decrease in product yield was observed. For *cis*-stilbene, the yield of the epoxide product was still lower and small amounts of *trans*-stilbene oxide were present together with benzophenone and diphenylacetaldehyde. In the absence of oxygen, a small fraction of *trans*-stilbene was detected, which indicates that some *cis* ⇌ *trans* isomerization of the olefin may have occurred either thermally or via exposure of the sample to light during the course of the reaction.

The products of the reactions between $Ru^{IV}=O^{2+}$ and norbornene or styrene were determined qualitatively by ^{1}H-NMR spectroscopy. In the case of norbornene the only product observed was the *exo*-norbornene oxide (6.85 ppm), while for styrene the styrene oxide (2.76, 3.12, 3.84 ppm) was obtained with no evidence for the formation of benzaldehyde. It is possible that GC-MS product analysis might have revealed other, minor products in addition to the epoxides but this was not pursued.

^{18}O-Labeling Analysis. In order to determine the source of the oxygen in the epoxide products two ^{18}O-labeling experiments were conducted. The first reaction involved a 1:1 mixture of $Ru^{IV}=^{18}O^{2+}$ and *trans*-stilbene. The amount of ^{18}O in the products was determined by GC-MS analysis. In an aerated solution, there was 80% transfer of the ^{18}O label to the epoxide and 54% transfer to benzophenone. When the reaction was performed under argon the fraction of ^{18}O-transfer increased to >87% in the epoxide and >63% in benzophenone. Subsequently, the $Ru^{IV}=^{18}O^{2+}$ sample used for the latter experiment was found to have undergone partial exchange, suggesting that the transfer of the ^{18}O label to the epoxide may well have been quantitative. The second reaction involved a 1:1 mixture of $Ru^{IV}=O^{2+}$ and *trans*-stilbene with addition of excess $H_2{}^{18}O$. In this case, there was <1% of the ^{18}O label transferred to the epoxide and <5% to benzophenone.

Metal Complex Products. The final ruthenium product was $[Ru^{II}(bpy)_2(py)(NCCH_3)]^{2+}$ when the reactions were performed with a large excess of olefin. At or near stoichiometric conditions, an additional product appeared (λ_{max} ~ 640 nm, see Figure 6), which has been identified as the μ-oxo-bridged dimer, $[Ru^{III}(bpy)_2(py)]_2O^{4+}$, by comparison with an authentic sample. The complex undergoes slow solvolysis to give $[(bpy)_2(CH_3CN)Ru^{III}-O-Ru^{III}(py)(bpy)_2]^{4+}$,[17] so corrections were applied to the molar absorptivity value at 640 nm to account for the distribution between the two dimeric species at the time when the reaction mixtures were analyzed spectrophotometrically. The 1:1 reaction between $Ru^{IV}=O^{2+}$ (15 mM) and *trans*-stilbene (15 mM) resulted in the formation of 94.5% $Ru^{II}-NCCH_3{}^{2+}$ and 5.5% Ru_2O^{4+}. When a 1:4 ratio of $Ru^{IV}=O^{2+}$ (3.75 mM) to *trans*-stilbene (15 mM) was used, the fraction of Ru_2O^{4+} decreased to 2.7% while the remainder (97.3%) was $Ru^{II}-NCCH_3{}^{2+}$. Similarly, the 1:1 reaction between $Ru^{IV}=O^{2+}$ (15 mM) and *cis*-stilbene (15 mM) resulted in the formation of 96% $Ru^{II}-NCCH_3{}^{2+}$ and 4% Ru_2O^{4+}.

Overoxidation Products. In Figure 7 are shown the UV–vis spectral changes with time for the 1:1 reaction between $Ru^{IV}=O^{2+}$ (13 mM) and *trans*-stilbene oxide (13 mM) in CH_3CN at room temperature. In comparison to the reaction with *trans*-stilbene, there was enhanced formation (~30%) of the μ-oxo-bridged dimer $[Ru^{III}(bpy)_2(py)]_2O^{4+}$ (λ_{max} = 640 nm) and the final Ru(II) product appeared to be $[Ru(bpy)_2(py)(NCCH_3)]^{2+}$ (λ_{max} = 440 nm). The GC-MS analysis of the organic products from this reaction revealed the formation of 6% benzophenone, 10% diphenylacetaldehyde, and 84% unreacted *trans*-stilbene oxide. The following observations were made: (a) once formed the epoxide is susceptible to further oxidation; (b) *overoxidation* of the epoxide forms the same non-epoxide products as observed in the epoxidation of *trans*-stilbene; (c) *overoxidation* of the epoxide is slower than oxidation of *trans*- stilbene but the time scales overlap; and (d)

(17) Doppelt, P.; Meyer, T. J. *Inorg. Chem.* **1987**, *26*, 2027.

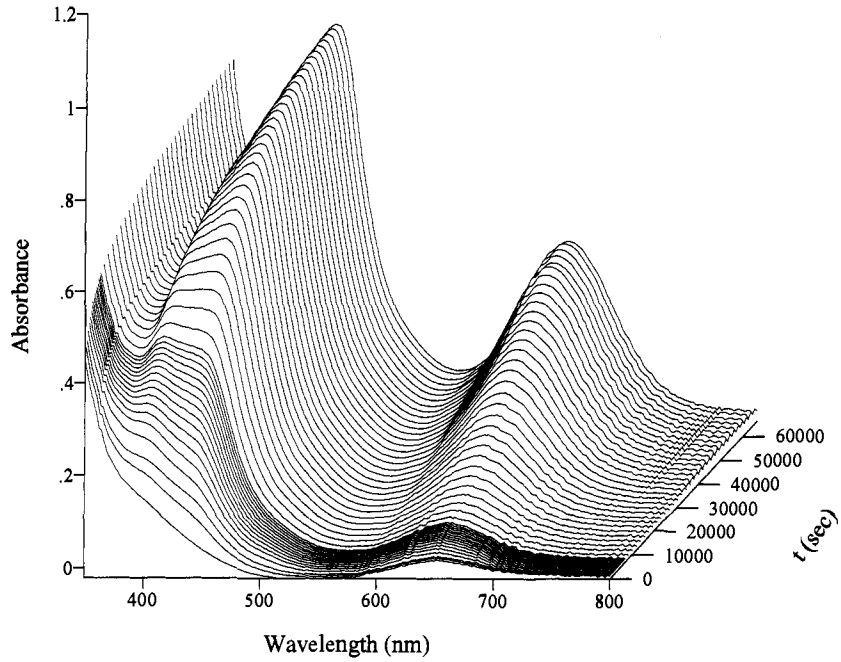

Figure 6. UV−vis spectral changes observed for the reaction between 13 mM $[Ru^{IV}(bpy)_2(py)(O)]^{2+}$ and 13 mM *trans*-stilbene in CH_3CN solution at $T \sim 25$ °C, path length = 0.01 cm.

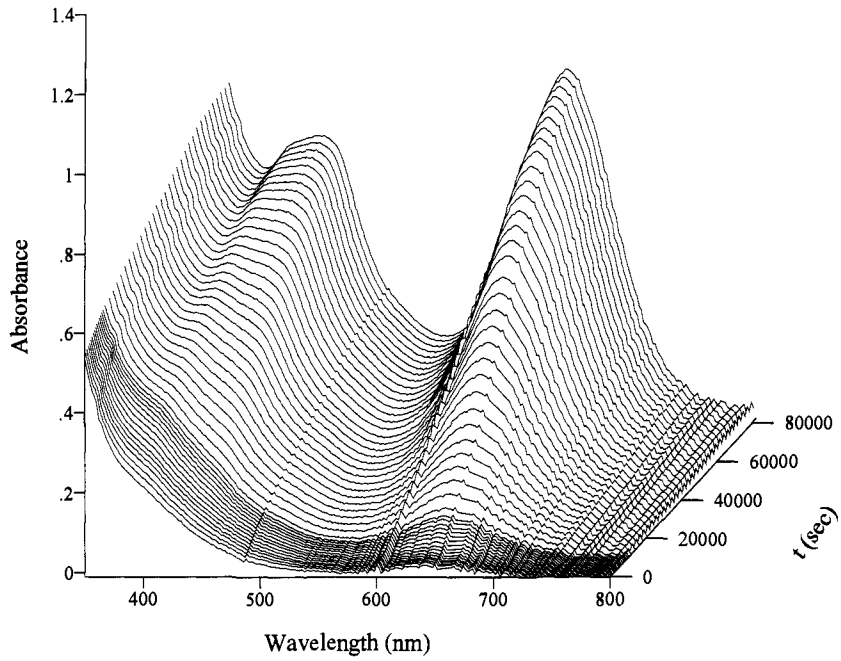

Figure 7. UV−vis spectral changes observed for the reaction between 13 mM $[Ru^{IV}(bpy)_2(py)(O)]^{2+}$ and 13 mM *trans*-stilbene oxide in CH_3CN solution at $T \sim 25$ °C, path length = 0.01 cm.

overoxidation consumes a large number of redox equivalents (~5) based on the amount of unreacted epoxide.

Kinetics. The oxidations of *cis*- and *trans*-stilbene, styrene, and norbornene by $Ru^{IV}{=}O^{2+}$ were followed under pseudo-first-order conditions with a large excess of olefin. In the case of *trans*-stilbene it was possible to obtain the rate constant for the initial step by kinetic measurements at 388 nm. This is an isosbestic wavelength for the loss of $Ru^{III}{-}OH^{2+}$ in the second stage of the reaction, allowing the kinetics of the Ru(IV) → Ru(III) stage to be studied with only slight interference from following reactions. Under these conditions the kinetics could be fit by using the programs MINSQ[18] or KINFIT[19] to a biexponential rate law (eq 4) for a reaction of the type A → B → C, where A_t and A_∞ are the absorbances at times t and ∞, respectively, α and β are absorbance amplitudes, and the rate constants are k_α and k_β.

$$|A_t - A_\infty| = \alpha e^{(-k_\alpha t)} + \beta e^{(-k_\beta t)} \quad (4)$$

The value of the faster rate constant, k_α (s^{-1}), varied linearly with olefin concentration over at least a 10-fold range, while k_β remained relatively invariant. The second-order rate constant for epoxidation was obtained by use of eq 5, which includes a stoichiometric factor of 2 in order to account for the additional consumption of the $Ru^{IV}{=}O^{2+}$ oxidant by rapid reaction with the Ru(II) epoxide product (eq 3), as inferred from the spectral

(18) *MINSQ Nonlinear Parameter Estimation and Model Development*; MicroMath Scientific Software: Salt Lake City, 1991.

(19) *KINFIT Nonlinear Curve Fitting For Kinetic Systems*; Binstead, R. A.; Chemistry Department, University of North Carolina: Chapel Hill, NC, 1990.

Table 2. Rate Constants for Epoxidation by $[Ru^{IV}(bpy)_2(py)(O)]^{2+}$ in CH_3CN

olefin	T, °C	[olefin]$_0$, M	10^3k_{obsd} s^{-1}[a]	$10^3k'$ M^{-1} s^{-1}[b]
trans-stilbene[c]	15.0	0.0306	19.5 ± 0.5	240 ± 6
	25.0	0.0234	14.9 ± 0.1	319 ± 2
	34.9	0.0408	33.7 ± 0.4	413 ± 5
	44.6	0.0405	45.0 ± 0.3	556 ± 4
	54.9	0.0400	55.2 ± 0.8	690 ± 10
cis-stilbene[d]	18.5	0.168	0.541 ± 0.004	1.61 ± 0.01
	25.0	0.080	0.414 ± 0.003	2.59 ± 0.02
	25.0	0.160	0.835 ± 0.008	2.61 ± 0.03
	25.0	0.250	1.214 ± 0.040	2.43 ± 0.08
	35.2	0.159	1.648 ± 0.006	5.18 ± 0.02
	42.5	0.158	2.596 ± 0.014	8.22 ± 0.04
	50.1	0.159	4.305 ± 0.050	13.5 ± 0.08
styrene[d]	25.0	0.0655	2.12 ± 0.01	
	25.0	0.327	9.92 ± 0.05	
	25.0	0.655	20.3 ± 0.2	15.4 ± 0.3[e]
norbornene[d]	25.0	0.0150	0.153 ± 0.009	
	25.0	0.0460	0.614 ± 0.004	
	25.0	0.2098	2.79 ± 0.02	
	25.0	0.4195	5.48 ± 0.04	6.56 ± 0.07[e]

[a] Only k_{obsd} (s^{-1}) for the initial step in the reaction is reported (see text). [b] $k' = k_{obsd}/(2[olefin]_0)$, corrected for the stoichiometry of the reaction (see text). [c] Obtained from single-wavelength kinetic fits at 388 nm to a biexponential rate law. [d] Obtained from global kinetic fits of the data (350–550 nm) to multiexponential rate laws. [e] Obtained from a linear fit of k_{obsd} *vs* [olefin].

changes. The results of the kinetic studies are summarized in Table 2.

$$k' = \frac{k_\alpha}{2[\text{olefin}]_0} \quad (5)$$

The kinetics for oxidation of *cis*-stilbene, styrene, and norbornene were better represented by a triexponential rate law for a reaction of the type A → B → C → D. In these cases, the entire spectral data set was processed in the SPECFIT program. Although a highly simplified model for these reactions, it was adequate for isolating the rate constants for the initial epoxidation step. In the case of *cis*-stilbene, the fastest of the rate constants accounted for only a small fraction of the total absorbance change and was ascribed to reduction of $Ru^{IV}{=}O^{2+}$ by impurities. The second rate constant in this scheme varied linearly with the concentration of *cis*-stilbene over the range 0.080–0.250 M (Table 2). At lower concentrations there was too much temporal overlap with following reactions to obtain a meaningful fit. In the case of styrene (0.0655–0.655 M) or norbornene (0.015–0.42 M) the fastest of the rate constants was found to depend linearly on olefin concentration over at least a 10-fold range. The second-order rate constants for these reactions are also listed in Table 2.

Activation parameters for the first step in the epoxidations of *trans*- and *cis*-stilbene by $Ru^{IV}{=}O^{2+}$ in CH_3CN were determined over the temperature ranges 15.0–54.9 and 18.5–50.1 °C, respectively. In accordance with the Eyring relationship, plots of the rate constants in Table 2 as $\ln(k'/T)$ *vs* $1/T$ were linear and from the slope and intercept the activation parameters were calculated to be $\Delta H^\ddagger = 4.4 \pm 0.1$ kcal mol^{-1} and $\Delta S^\ddagger = -46 \pm 0.4$ cal deg^{-1} mol^{-1} for *trans*-stilbene and $\Delta H^\ddagger = 11.9 \pm 0.1$ kcal mol^{-1} and $\Delta S^\ddagger = -30.4 \pm 0.3$ cal deg^{-1} mol^{-1} for *cis*-stilbene.

Discussion

Epoxidation of *trans*-Stilbene. Singular value decomposition of the wavelength–time data matrices for the reduction of $[Ru^{IV}(bpy)_2(py)(O)]^{2+}$ by large excesses of *cis*- and *trans*-stilbene, styrene, and norbornene each revealed five significant sets of eigenvectors, implying a minimum of four distinct kinetic processes. Although strikingly similar in overall behavior, only in the case of *trans*-stilbene was the initial stage of the reaction sufficiently rapid to separate the formation and decay of the intermediates. This allowed the successful application of global kinetic analysis methods to extract details about each stage of the epoxidation reaction, as presented below.

Mechanism of the Initial Stage. The available evidence suggests that initial $Ru^{IV}{=}O^{2+}$ oxidation of *trans*-stilbene occurs by:

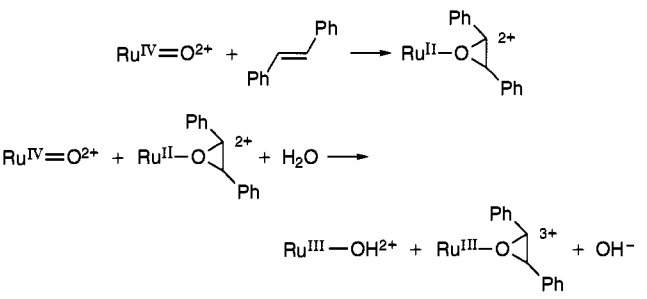

The rate law is first order in $Ru^{IV}{=}O^{2+}$ and *trans*-stilbene and is independent of added water over the range 10–450 mM. The hydroxide ion appearing in this scheme is demanded by the mechanism for proton balance. The acetonitrile used was not predried and typically contained ~10 mM (0.02% w/v) water.[20] The spectral changes at early times (~60 s) show that the initial $Ru^{IV}{=}O^{2+}$ is converted into species whose spectra resembled $Ru^{III}{-}OH^{2+}$. The addition of excess ascorbic acid at this stage gave two separate Ru(II) species, both of which solvolyzed to $Ru^{II}{-}NCCH_3^{2+}$ but at different rates. One of the species was identified as $Ru^{II}{-}OH_2^{2+}$ from both the predicted spectrum and solvolysis rate constant (1.6×10^{-3} s^{-1}) returned by a global fit of the data to the kinetic model A → C, B → C. The Ru(II) form of the second intermediate solvolyzed much more rapidly ($k = 0.42 \pm 0.05$ s^{-1}) and is presumed to be the Ru(II) epoxide complex.

Careful inspection of the data in Figure 1 shows that in the initial stage of the reaction there is evidence for small amounts of both $Ru^{II}{-}OH_2^{2+}$ and $Ru^{II}{-}NCCH_3^{2+}$. The early appearance of $Ru^{II}{-}NCCH_3^{2+}$ results from solvolysis of both the aqua complex and the Ru(II) epoxide intermediate,

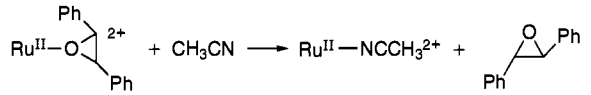

However, rapid reoxidation of $Ru^{II}(epoxide)^{2+}$ by $Ru^{IV}{=}O^{2+}$ (eq 3) competes with solvolysis to such an extent that only a small fraction of free epoxide is formed in the initial stage. Solvolysis of $Ru^{II}(epoxide)^{2+}$ only plays an important role once the concentration of $Ru^{IV}{=}O^{2+}$ has fallen significantly.

Mechanism of the Second Stage. In the presence of excess olefin, a series of overlapping steps leads to the disappearance of the Ru(III) intermediates and the formation of $Ru^{II}{-}NCCH_3^{2+}$.

I. Recycling of $Ru^{III}{-}OH^{2+}$. Once formed, $Ru^{III}{-}OH^{2+}$ is in rapid equilibrium with $Ru^{IV}{=}O^{2+}$ and $Ru^{II}{-}OH_2^{2+}$ (eq 2). This creates a "feedback loop" for further production of

(20) The water content of samples of the acetonitrile used for the kinetic studies was determined by FT-IR analysis.

(21) (a) Lever, A. B. P. *Inorg. Chem.* **1990**, *29*, 1271. (b) Suem, H. F.; Wilson, S. W.; Pomerantz, M.; Walsh, J. L. *Inorg. Chem.* **1989**, *28*, 786. (c) Brown, G. M.; Callahan, R. W.; Meyer, T. J. *Inorg. Chem.* **1975**, *14*, 1915.

the epoxide via the reactions shown above. The aqua complex subsequently undergoes irreversible solvolysis by CH_3CN (eq 1c).[16]

II. Release of Epoxide. It is not clear from the spectral observations how the bulk of the epoxide is released into solution. One possibility is by solvolysis of $Ru^{III}(epoxide)^{3+}$,

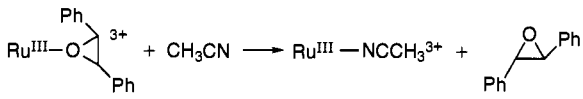

This would give $[Ru^{III}(bpy)_2(py)(NCCH_3)]^{3+}$, which is a powerful oxidant ($E_{1/2} = +1.6$ V *vs* NHE)[21] capable of rapid oxidation of $Ru^{II}-OH_2^{2+}$, $Ru^{III}-OH^{2+}$, the excess olefin, or the epoxide itself. Given the absence of ^{18}O in the epoxide product when the reaction is performed in the presence of excess $H_2{}^{18}O$, epoxidation does not occur to any significant degree by the reaction,

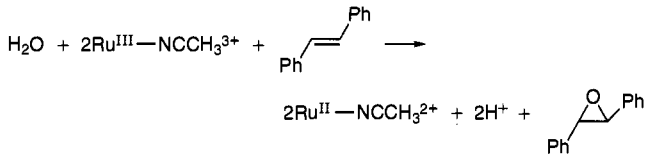

A small contribution from one-electron oxidation of the olefin by $Ru^{III}-NCCH_3^{3+}$ could explain the slight decrease in the extent of ^{18}O transfer and the slightly increased yield of oxidation products in the presence of O_2 (Table 1). These suggest that O_2 is an auxiliary oxidant in the second stage of the reaction induced by pathways such as,

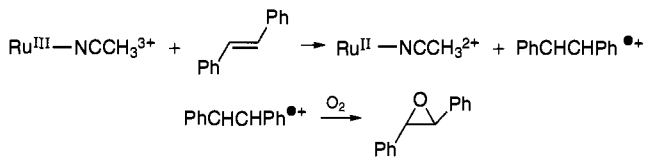

This could explain the formation of a small amount of *trans*-stilbene oxide from *cis*-stilbene. However, a more plausible explanation for the latter is the formation of a small amount of *trans*-stilbene via *cis* ⇌ *trans* isomerization during the course of the reaction. *trans*-Stilbene is ~100 times more reactive toward oxidation than *cis*-stilbene (Table 2).

Kinetic Model. The results of the product analyses, quenching studies, and the factor analysis of the spectral changes for the reaction between *trans*-stilbene and $[Ru^{IV}(bpy)_2(py)(O)]^{2+}$ in CH_3CN are consistent with the following model.

$$Ru^{IV}{=}O^{2+} + \text{olefin} \xrightarrow{k_1} Ru^{II}(\text{epoxide})^{2+} \quad (6a)$$

$$Ru^{IV}{=}O^{2+} + Ru^{II}(\text{epoxide})^{2+} + H_2O \xrightarrow[rapid]{k_2} Ru^{III}{-}OH^{2+} + Ru^{III}(\text{epoxide})^{3+} + OH^- \quad (6b)$$

$$2\,Ru^{III}{-}OH^{2+} \underset{k_4}{\overset{k_3}{\rightleftharpoons}} Ru^{IV}{=}O^{2+} + Ru^{II}{-}OH_2{}^{2+} \quad (6c)$$

$$Ru^{II}(\text{epoxide})^{2+} + CH_3CN \xrightarrow{k_5} Ru^{II}{-}NCCH_3{}^{2+} + \text{epoxide} \quad (6d)$$

$$Ru^{II}{-}OH_2{}^{2+} + CH_3CN \xrightarrow{k_6} Ru^{II}{-}NCCH_3{}^{2+} + H_2O \quad (6e)$$

$$Ru^{III}(\text{epoxide})^{3+} + CH_3CN \xrightarrow[+e^-]{k_7} Ru^{II}{-}NCCH_3{}^{2+} + \text{oxidation products} \quad (6f)$$

This sequence of reactions explains the presence of two forms of Ru(III) after the initial loss of the $Ru^{IV}{=}O^{2+}$ oxidant and the slow appearance of the final solvento complex, $Ru^{II}-NCCH_3{}^{2+}$, via disproportionation of $Ru^{III}-OH^{2+}$. It also explains the appearance of small amounts of $Ru^{II}-OH_2{}^{2+}$ and $Ru^{II}-NCCH_3{}^{2+}$ formed in the initial stage of the reaction. As discussed above, the loss of Ru(III) epoxide may occur by solvolysis and subsequent reduction of $Ru^{III}-NCCH_3{}^{3+}$. Other possibilities that cannot be excluded by the data include the following: (a) an intramolecular electron transfer to form an epoxide radical; or (b) reduction by excess olefin to give a stilbene radical and the Ru(II) epoxide, followed by rapid solvolysis. These are kinetically indistinguishable.

Refinement Scheme. The complexity of the kinetic scheme mandated a global least-squares fit of the kinetic–spectral data with the SPECFIT program to model the reaction scheme with the use of a stiff numerical integration method. Several stages of the reaction were studied independently to obtain rate constants and spectra that could be held constant during the refinement of the full kinetic model.

I. The solvolysis of $[Ru^{II}(bpy)_2(py)(OH_2)]^{2+}$ in acetonitrile at 25 °C has been studied previously by diode array kinetics, yielding the rate constant, $k_6 = (1.66 \pm 0.02) \times 10^{-3}$ s^{-1}, and the predicted spectra of the aqua and acetonitrile complexes from a global least-squares fit.[16]

II. The disproportionation of $[Ru^{III}(bpy)_2(py)(OH)]^{2+}$ in acetonitrile at 25 °C also has been studied previously by a combination of rapid-scan, stopped-flow kinetics (OLIS RSM/1000) for the comproportionation step and diode array kinetics for the slow disproportionation and solvolysis stages. Global fits returned the rate constants, $k_3 = 80.6 \pm 0.4$ M^{-1} s^{-1} and $k_4 = 4070 \pm 130$ M^{-1} s^{-1}, and the predicted spectrum of $Ru^{III}-OH^{2+}$.[16]

III. The solvolysis of $[Ru^{II}(bpy)_2(py)(epoxide)]^{2+}$ in acetonitrile at 25 °C was studied following quenching of the reaction after 1 min by 1:1 mixing with a saturated solution of ascorbic acid. The solvolysis was followed by rapid-scan, stopped-flow kinetics. Interference from the slower solvolysis of the coproduct, $Ru^{II}-OH_2{}^{2+}$, was a minor problem but the global fits still gave a reasonably precise estimate of $k_5 = 0.42 \pm 0.05$ s^{-1}. The accuracy of this value is not of great importance in the fit to the full kinetic model since both solvolysis and reoxidation prevent the observation of the Ru(II) epoxide complex at any stage of the reaction.

IV. Successful least-squares refinement to the full kinetic model was obtained by use of the SPECFIT program with known molar absorptivity spectra for $Ru^{IV}{=}O^{2+}$, $Ru^{III}-OH^{2+}$, $Ru^{II}-OH_2{}^{2+}$, and $Ru^{II}-NCCH_3{}^{2+}$ as constraints to the fit. Only the spectra of the Ru(III) epoxide and excess, free *trans*-stilbene were allowed to vary in the fit. The combination of known spectra and measured rate constants for several steps in the overall scheme was critical to obtaining a meaningful solution to the kinetic scheme. The refined values of the remaining rate constants are given in Table 3. The spectral components and concentration profiles obtained from the global fit for the oxidation of *trans*-stilbene are shown in Figure 8.

Similar results were obtained for a range of concentrations of *trans*-stilbene (0.02–0.08 M), with some variation in k_7. The temporal overlap of the various kinetic processes worsens with decreasing olefin concentration, increasing the cross-correlation between the adjustable parameters. Therefore, the variation in

Table 3. Parameters from the Global Refinement to the Kinetic Model for Reduction of 6.4 × 10^{-5} M $[Ru^{IV}(bpy)_2(py)(O)]^{2+}$ by 0.080 M *trans*-Stilbene in CH_3CN at 25 °C

reaction	rate constant	parameter type	fixed parameter source
k_1 (M^{-1} s^{-1})	(2.78 ± 0.02) × 10^{-1}	adjustable	
k_2 (M^{-1} s^{-1})[a]	(3.29 ± 0.23) × 10^{5}	adjustable	
k_3 (M^{-1} s^{-1})	(8.06 ± 0.04 × 10^{1}	fixed	disproportionation[b]
k_4 (M^{-1} s^{-1})	(4.07 ± 0.13) × 10^{3}	fixed	comproportionation[b]
k_5 (s^{-1})[a]	(0.42 ± 0.05)	fixed	quenching/solvolysis[c]
k_6 (s^{-1})	(1.66 ± 0.02) × 10^{-3}	fixed	solvolysis[b]
k_7 (s^{-1})	(2.46 ± 0.02) × 10^{-4}	adjustable	

[a] k_2 and k_5 are highly correlated parameters since the reactions are competitive. [b] Parameters obtained from independent global least-squares fits (see ref 16). [c] Parameter obtained in this work from quenching studies (see text).

k_7 was not considered to be significant since a single set of parameters (Table 3) gave equally good fits to each data set.

Epoxidation. For each of the olefins the initial stage of epoxidation was first order in both olefin and oxidant. For *trans*-stilbene the rate constants obtained from the global kinetic analysis (k_1 = 0.28−0.30 M^{-1} s^{-1} at 25 °C) agreed well with the value obtained from single-wavelength fits at 388 nm (k_1 = 0.32 M^{-1} s^{-1}). Even given the mechanistic complexities and overlap between steps it is noteworthy that the same model and rate constants correctly fit the appearance of $[Ru^{II}(bpy)_2(py)(NCCH_3)]^{2+}$ for *cis*-stilbene, even though the initial step (k_1) is ~100 times slower (Table 2). The rate of appearance of the solvento complex is independent of both the concentration and the stereochemistry of the reductant and appears to be dominated by the kinetics of disproportionation of $Ru^{III}-OH^{2+}$. For styrene and norbornene there is less evidence for the involvement of $Ru^{III}-OH^{2+}$ and the extent of reoxidation of the initial Ru(II) epoxide product is unknown.

Overoxidation of the Epoxide. A further complication exists from oxidation of the epoxide once it is formed. This is illustrated by the stoichiometric reaction between 13 mM $Ru^{IV}=O^{2+}$ and 13 mM *trans*-stilbene oxide (Figure 7), in which the major organic products are diphenylacetaldehyde, which is an isomer of the epoxide, and benzophenone (Table 1). By inference, the formal loss of a CH_2 unit from the initial epoxide to form benzophenone implies the consumption of further redox equivalents. Presumably, this results in the formation of CH_3OH, HCOOH, or CO_2, none of which could be detected with the GC-MS technique with acetonitrile as the solvent. In addition, a characteristic feature of the overoxidation reaction is the appearance of ~30% of the μ-oxo dimer Ru_2O^{4+}. Similar behavior was observed for the stoichiometric oxidation of *trans*-stilbene (Figure 6) except that the yield of Ru_2O^{4+} was lower.

Given the appearance of benzophenone, it is presumed that overoxidation involves initial epoxide → epoxide• radical formation. The appearance of Ru_2O^{4+} as a product indicates that, to at least a small degree, O-atom transfer must occur to the radical followed by attack of a second $Ru^{IV}=O^{2+}$ to produce a μ-oxo core. This point requires further investigation. The source of the oxidative equivalents for overoxidation could be $Ru^{IV}=O^{2+}$, $Ru^{III}-OH^{2+}$, $Ru^{III}(epoxide)^{3+}$, or $Ru^{III}-NCCH_3{}^{3+}$ or contributions from all four. Overoxidation is expected to play a major role at or near stoichiometric conditions. Under conditions of excess olefin, as used for the kinetic studies, overoxidation is presumably not competitive. Unfortunately, we were unable to determine product distributions with a large excess of olefin present so this point remains unresolved.

Miller and co-workers have shown that the products of electrochemical oxidation of *trans*-stilbene oxide are benzophenone and diphenylacetic acid.[22] One-electron oxidation of the epoxide by Ru(III) may be responsible for the formation of benzophenone (andpresumably CO_2) as shown below based on Ru(III) as the oxidant.

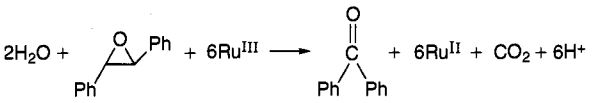

The details of the reaction are unknown. Given the initial and final products, there must be a phenyl transfer in a radical intermediate which implies

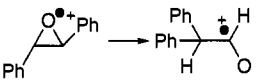

This step, followed by further oxidation, would explain the trace of aldehyde detected in our experiments and the corresponding acid observed in the electrochemical experiment. A combined or sequential phenyl-H transfer to give

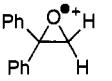

followed by further oxidation by Ru(IV), Ru(III), and/or O_2 would give benzophenone and CO_2 after further oxidation of the CH_2 fragment.

There may also be a contribution to the pool of radical products from the $Ru^{III}(epoxide)^{3+}$ intermediate by initial intramolecular oxidation rather than solvolysis,

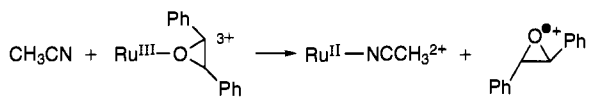

Subsequent oxidation of the epoxide radical by $Ru^{IV}=O^{2+}$ or $Ru^{III}-OH^{2+}$ would lead to benzophenone and CO_2. Bruice *et al.* have also reported overoxidation of *cis*-stilbene oxide by Cr^{V}(oxometalloporphyrins) to give diphenylacetaldehyde and benzaldehyde.[23]

Mechanism of Epoxidation. A number of mechanisms have been proposed for epoxidation of olefins by metalloporphyrins via metal oxo intermediates.[1,2] They include the following: (1) initial metallaoxetane formation; (2) one-electron oxidation to give either σ-carbon or π-cation radical intermediates; (3) net two-electron O-atom transfer via carbocation intermediates; and (4) concerted oxene insertion to form the epoxide directly. Based on the results of our kinetic studies, epoxidation of the olefins by $Ru^{IV}=O^{2+}$ is first order in each reactant to give $Ru^{II}(epoxide)^{2+}$ without evidence for intermediates. The ^{18}O-labeling experiments with $Ru^{IV}={}^{18}O^{2+}$ and $H_2{}^{18}O$ show that oxygen atom transfer from the oxidant is the primary source of oxygen in the epoxide.

Cundari and Drago have studied the interaction of six-coordinate Ru(IV)−oxo complexes with olefins to form epoxides by using INDO/1 calculations.[24] After the reactants have passed a small activation barrier for association (at ≈2.7 Å), their results favor a non-concerted [1 + 2] pathway in which the olefin approaches the metal−oxo bond in an off-center orientation (Scheme 1). This decreases the repulsion between the oxo lone pair (largely p_z) and the ethylene π MO while increasing the interaction between ethylene and Ru−oxo π

(22) Mayeda, E. A.; Miller, L. L.; Wolf, J. F. *J. Am. Chem. Soc.* **1972**, *94*, 6812.

(23) (a) Garrison, J. M.; Bruice, T. C. *J. Am. Chem. Soc.* **1989**, *111*, 191. (b) Garrison, J. M.; Ostovic, D.; Bruice, T. C. *J. Am. Chem. Soc.* **1989**, *111*, 4960.

(24) Cundari, T. R.; Drago, R. S. *Inorg. Chem.* **1990**, *29*, 487.

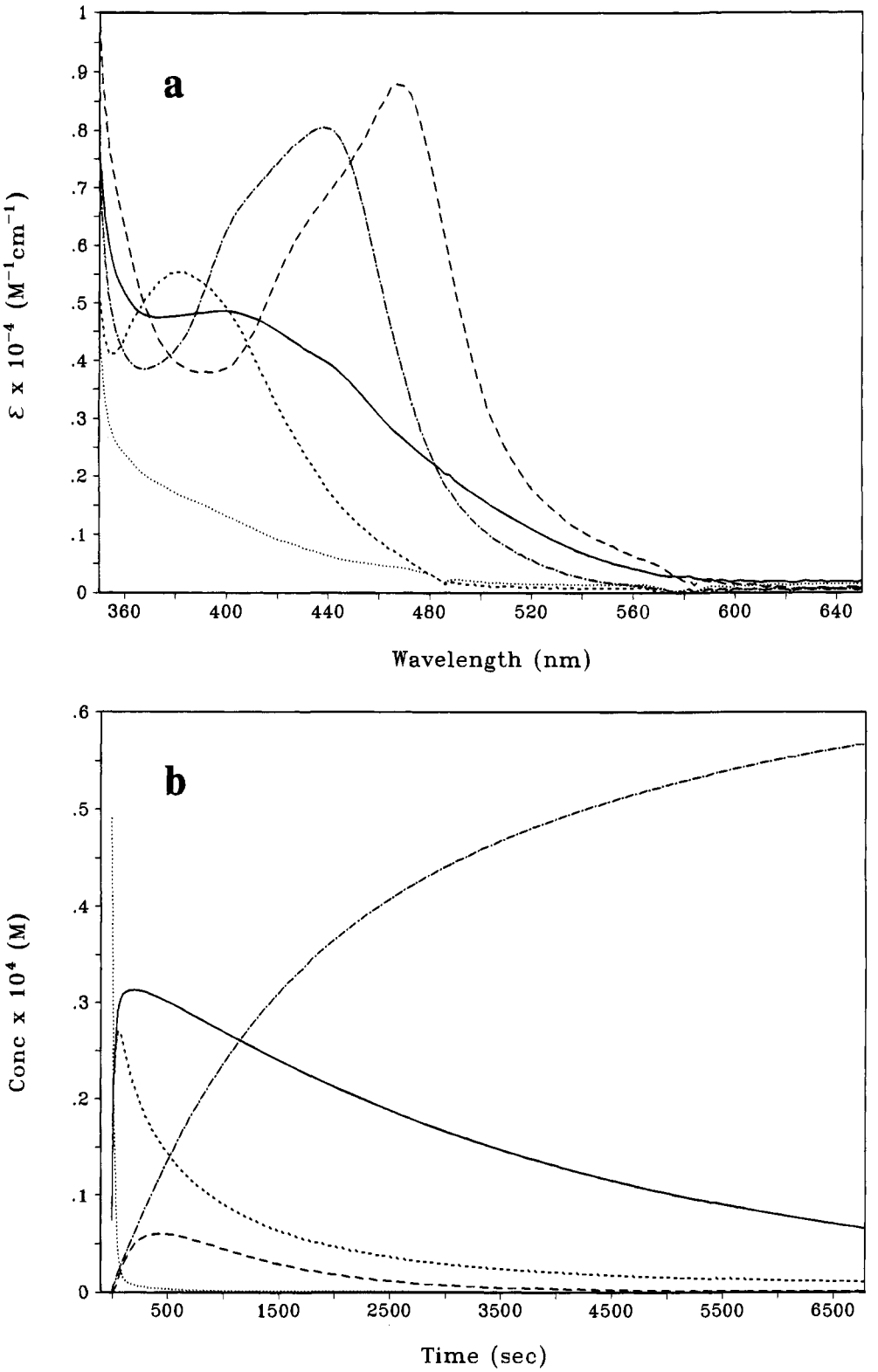

Figure 8. (a) Predicted UV−vis molar absorptivity spectrum for $[Ru^{III}(bpy)_2(py)(O\text{-stilbene})]^{3+}$ (—), and the constrained spectra for $[Ru^{IV}(bpy)_2(py)(O)]^{2+}$ (•••), $[Ru^{III}(bpy)_2(py)(OH)]^{2+}$ (- - -), $[Ru^{II}(bpy)_2(py)(OH_2)]^{2+}$ (— —), and $[Ru^{II}(bpy)_2(py)(NCCH_3)]^{2+}$ (— • —) in CH_3CN solution at T = 25.0 ± 0.2 °C. (b) Predicted concentration profiles obtained for these species from the global fit of the spectral−kinetic data in Figure 1 to the kinetic model for epoxidation, as given in the text.

MO's, as well as the back-bonding from the oxo σ lone pair to the ethylene π^* MO. The pathway is non-concerted in that the first C−O bond of the epoxide is almost entirely formed before the second C−O bond begins to form. From a kinetic point of view, the reaction may appear to be concerted if the formation of the second C−O bond is more rapid than the rotation of the C−C bond, which would lead to the loss of stereochemistry for *cis*-stilbene. Our results show only a minor loss of stereochemistry for *cis*-stilbene to give the thermodynamically favored *trans*-stilbene oxide, but we believe this is due to isomerization of the olefin during the course of the reaction rather than to rotation of the C−C bond during intermediate formation.

The INDO/1 results also show a preference for an off-perpendicular, canted approach of the ethylene fragment to the vector describing the Ru−O bond as shown in Scheme 1. This

Scheme 1

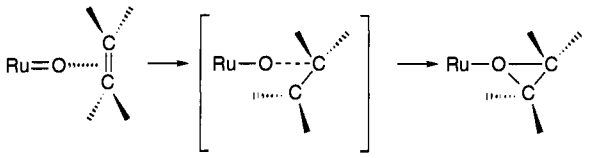

Table 4. Rate Constants and Activation Parameters for Selected Oxygen Atom Transfer Reactions of $[Ru^{IV}(bpy)_2(py)(O)]^{2+}$ in CH_3CN

reductant	T, °C	k, M^{-1} s^{-1}	$\Delta H^{\ddagger}$, kcal mol^{-1}	$\Delta S^{\ddagger}$, cal deg^{-1}	ref
PPh_3	19	1.33×10^5	4.7 ± 0.5	-19 ± 3	5
C_6H_5OH	25	1.9×10^2	10.3 ± 0.6	-14 ± 2	7
$S(CH_3)_2$	25	1.71×10^1	8.0 ± 0.8	-26 ± 3	4
$OS(CH_3)_2$	25	1.34×10^{-1}	6.8 ± 0.2	-39 ± 3	4
trans-stilbene[a]	25	2.8×10^{-1}	4.4 ± 0.1	-46 ± 0.4	this work
cis-stilbene[a]	25	2.5×10^{-3}	11.9 ± 0.1	-30.4 ± 0.3	this work

[a] Activation parameters were obtained from single determinations at each temperature. The small standard errors from the fits may be underestimates.

increases the overlap between the ethylene and Ru−oxo π symmetry orbitals. In the case of nonplanar *cis*-stilbene, the combination of the off-center and canted approaches leads to unfavorable steric repulsions with the phenyl rings in the organic fragment. The steric barrier is significantly smaller for the planar *trans*-stilbene isomer. Steric repulsion probably accounts for the slower rate constant for the formation of the *cis*-epoxide compared to the *trans* isomer. This is in contrast to porphyrin based oxidants where steric interactions with the planar porphyrin ring have been invoked to explain the slower rate of epoxidation of *trans*-stilbene compared to *cis*-stilbene.[25]

The activation parameters for *cis*- and *trans*-stilbene are shown in Table 4 along with examples of other O-atom transfer reactions based on $[Ru^{IV}(bpy)_2(py)(O)]^{2+}$. Although these reactions all proceed via "oxygen atom" transfer, the variations in activation parameters indicate that the intimate details of the various reactions may differ considerably with the reductant. They may depend on both electronic and steric properties.

Implications for Synthesis. The mechanistic studies reported here are revealing as to the possible use of $Ru^{IV}=O^{2+}$ and related oxidants in synthesis. They offer some important advantages. Kinetically, $Ru^{IV}=O^2$ is a relatively facile oxidant, comparable to Cr^V in $(Br_8TPP)Cr^VO(X)$,[23] even though it is of moderate oxidizing strength. The initial epoxidation step appears to be concerted, thus avoiding radical pathways and a multiplicity of products, if properly exploited. Once formed, $Ru^{II}(epoxide)^{2+}$ undergoes rapid solvolysis to liberate the epoxide, which is important for recycling the catalyst. However, in order to recycle the oxidant it is necessary for $Ru^{II}-OH_2^{2+}$ to reform so that it can undergo reoxidation by chemical or electrochemical means,

$$Ru^{II}-OH_2^{2+} \xrightarrow{2e^-} Ru^{IV}=O^{2+} + 2H^+$$

This is a well-established step, but it requires the presence of water and reformation of the aqua complex.

$$Ru^{II}(epoxide)^{2+} + H_2O \rightarrow Ru^{II}-OH_2^{2+} + epoxide$$

In coordinating solvents aquation is in competition with formation of the solvento complex. Under these conditions, the slow step can become aquation of the solvento complex formed by solvolysis of $Ru^{II}(epoxide)^{2+}$. For this reason acetonitrile is problematical as a reaction solvent, at least at room temperature, since it competes kinetically 1:18 with water in CH_3CN/H_2O mixtures.[16] Previous catalytic studies have been performed in biphasic CH_2Cl_2/H_2O mixtures to avoid this complication.

There is an equally important complication arising from rapid reoxidation of the labile $Ru^{II}(epoxide)^{2+}$ complex once it has formed. The oxidation of $Ru^{II}(epoxide)^{2+}$ to Ru(III) by $Ru^{IV}=O^{2+}$ is more rapid than solvolysis of $Ru^{II}(epoxide)^{2+}$ and this dominates the subsequent course of events. The formation of Ru(III) slows down the appearance of free epoxide, complicates the mechanism, introduces radical character, and may contribute to overoxidation as well. The problem arises from slow solvolysis of $Ru^{III}(epoxide)^{3+}$ and the fact that both it and $Ru^{III}-NCCH_3^{3+}$ are potent one-electron oxidants. An obvious and important general solution to the problem of comproportionation is by surface attachment of the oxidant so as to avoid diffusional pathways, an approach that we are pursuing.

A second important conclusion about synthesis to arise in our findings is the general problem of overoxidation of epoxide products once they are formed. Inspection of previous work on metal porphyrin catalyzed oxidations of olefins reveals that in many cases products characteristic of overoxidation (*i.e* benzaldehyde, diphenylacetic acid) have been reported and often cited as evidence for a radical mechanism for epoxidation. In many cases, these unwanted coproducts may have no relevance to the mechanism of epoxidation and arise instead from overoxidation of a free or coordinated epoxide product.

Acknowledgment. This work was supported the National Science Foundation under Grant No. CHE-9203311. Part of this work was supported by the National Institutes of Health through a postdoctoral fellowship for MSR under Grant No. 1-F32-GM12737-01A1. The authors also express their appreciation to Prof. Andreas D. Zuberbühler at the University of Basel for access to the global least-squares algorithms used in the development of the SPECFIT program and for continuing advice on the application of factor analytical methods to kinetic systems.

JA9423882

(25) (a) Groves, J. T.; Nemo, T. E. *J. Am. Chem. Soc.* **1983**, *105*, 5786. (b) Ostovic, D.; Bruice, T. C. *J. Am. Chem. Soc.* **1988**, *110*, 6906.